



# Influence of solution heating on the properties of PEDOT:PSS colloidal solutions and impact on the device performance of polymer solar cells

Bettina Friedel<sup>a,b,\*</sup>, Thomas J.K. Brenner<sup>b</sup>, Christopher R. McNeill<sup>b</sup>, Ullrich Steiner<sup>b</sup>, Neil C. Greenham<sup>b</sup>

<sup>a</sup> Institute of Solid State Physics, Graz University of Technology, Petersgasse 16, A-8010 Graz, Austria

<sup>b</sup> Cavendish Laboratory, Department of Physics, University of Cambridge, JJ. Thomson Avenue, Cambridge CB3 0HE, United Kingdom

## ARTICLE INFO

### Article history:

Received 26 April 2011

Received in revised form 30 June 2011

Accepted 3 July 2011

Available online 29 July 2011

### Keywords:

Organic solar cell

PEDOT:PSS

Phase transition

Particle size

## ABSTRACT

We have investigated the effects of temperature variation on colloidal solutions of the electrode polymer poly(3,4-ethylenedioxythiophene):poly(styrenesulfonic acid) (PEDOT:PSS) and its consequences for photovoltaic devices using conjugated polymer blends as the photoactive material. By variation of the PEDOT:PSS solution temperature between 20 and 90 °C we observed reversible temperature-dependent change in size of the PEDOT:PSS particles. This process is associated with temperature and concentration dependent phase transitions of the PSS electrolyte chains. We found optimum device performance, in particular high quantum efficiency and power conversion efficiency for solar cells, with PEDOT:PSS layers produced from 70 °C solutions. After consideration of film morphology, particle size, conductivity and work function, we conclude that improved device performance originates from enhanced conductivity in films deposited from heated solutions. While film conductivity increases monotonically with solution temperature, devices produced using solution temperatures greater than 70 °C suffer from the increased work function of the PEDOT:PSS layer.

© 2011 Elsevier B.V. All rights reserved.

## 1. Introduction

Solar cells based on conjugated polymers have shown a considerable increase in device efficiency over the last decade [1–3]. For achieving high efficiencies, a thin layer of the conductive polymer mixture PEDOT:PSS (poly(3,4-ethylenedioxythiophene):poly(styrenesulfonic acid)) (Fig. 1) at the hole-collecting electrode is typically used [4]. PEDOT:PSS is thought to be beneficial for device performance in a number of ways. It not only decreases the surface roughness of indium-tin oxide (ITO) transparent electrodes, reducing the number of shorts in the device, but also improves the selectivity of the anode due to the higher work

function relative to ITO, enhancing electron blocking and therefore maintaining higher open-circuit voltage [5]. Changing the properties of PEDOT:PSS, for example via addition of surfactants and organic solvents [6] or thermal annealing [7–9] has been extensively examined. Studies focusing on the interplay between PEDOT:PSS treatment and device performance of polymer solar cells [10,11] show that both thickness and annealing temperature of the PEDOT:PSS layer influence the device performance significantly. However, understanding the relationship between morphological and chemical changes on one side and photovoltaic properties on the other side is desirable for more efficient solar cells. The commonly used PEDOT:PSS solution is a complex materials system. In order to circumvent the poor solubility and infusibility of pure PEDOT, it is polymerized in the presence of water-soluble polyelectrolyte PSS that acts as a dopant and counterion, and facilitates the formation of a stable aqueous colloidal solution [12].

\* Corresponding author at: Institute of Solid State Physics, Graz University of Technology, Petersgasse 16, A-8010 Graz, Austria. Tel.: +43 316 873 8978; fax: +43 316 873 8466.

E-mail addresses: [bf245@cam.ac.uk](mailto:bf245@cam.ac.uk), [bfriedel@tugraz.at](mailto:bfriedel@tugraz.at) (B. Friedel).

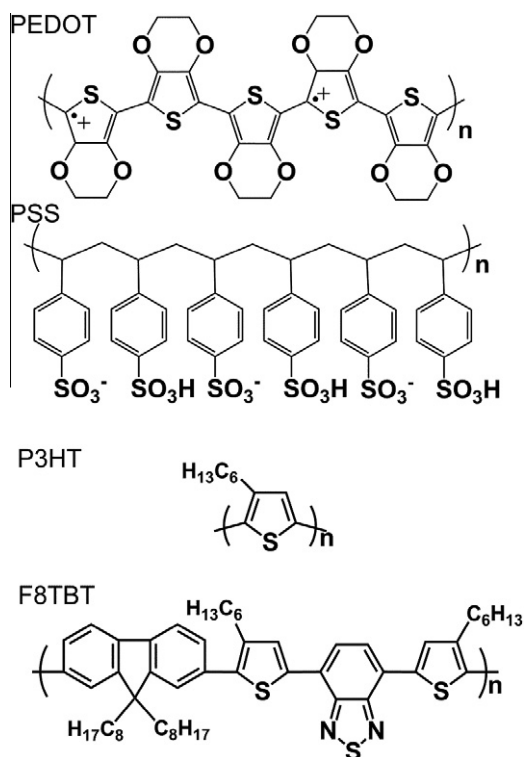


Fig. 1. Chemical structures of polymers used.

Generally these colloidal particles are described as entanglements of PSS chains with PEDOT oligomer units adsorbed to them. When in aqueous solution, the hydrophobicity of the adsorbed PEDOT causes preferential orientation of the hydrophilic sulfate groups to the outside and the PEDOT-rich parts of the chain to the inside of the entangled polymer chain, causing a micelle-like formation. From the macroscopic point of view this results in a particle with a PEDOT-rich conductive core and an insulating PSS-rich shell, which has been verified in numerous investigations on dried films, e.g. via XPS [5,13,14]. While the particles are in a swollen state when in aqueous solution, they shrink drastically during drying (water content up to ~95%) [12]. The PSS content in these solutions may be altered to tune the electric properties of PEDOT:PSS films. Up to a certain concentration, the PSS dopant enhances PEDOT:PSS film conductivity (up to ~10 S/cm). It decreases again for higher PSS content, due to the formation of PSS insulating cover layers or lamellae [15,16].

In this work we study the influence of thermal treatment on the PEDOT:PSS solution and resulting effects on the device performance of solar cells made from P3HT (poly(3-hexylthiophene)) and F8TBT (poly((9,9-dioctylfluorene)-2,7-diyl-alt-[4,7-bis(3-hexylthiophen-5-yl)-2,1,3-benzothiadiazole]-2',2''-diyl)) (Fig. 1) [17]. Besides electrical characterization of photovoltaic cells we employ photoelectron spectroscopy (both X-ray photoelectron spectroscopy (XPS) and ultraviolet photoelectron yield spectroscopy (PEYS)), atomic force microscopy (AFM) and electrical conductivity measurements to characterize solid PEDOT:PSS thin films, and ion activity measurement (pH)

and photon correlation spectroscopy (Dynamic Light Scattering (DLS)) on solutions to reveal the interplay between thermal treatment of PEDOT:PSS, resulting thin film properties and photovoltaic performance.

## 2. Experimental details

### 2.1. Materials

All substrates used (Spectrosil quartz glass, indium-tin oxide (ITO) coated sodium silicate glass) were cleaned by sonication in acetone and isopropanol (20 min. each), followed by oxygen plasma etching (250 W, 10 min). The aqueous colloidal PEDOT:PSS solution used has a PEDOT-to-PSS ratio of 1:16 (Clevios P VP Al 4083, H.C. Starck GmbH, subsequently enriched with PSS). Its nominal solid content is 2.2% and the particle size in the swollen state (in solution) is characterized by  $d_{50}$  of 80 nm and  $d_{90}$  of 100 nm ( $d_n$  implies that  $n$  wt.% of the particles are below the given size). The molecular weight of PSS in Clevios P is  $M_w = 313,000$  and  $M_n = 134,000$ . The aqueous PSS solution (Scientific Polymer Products Inc.) has a solid content of 20 wt.% and the PSS a molecular weight of  $M_w = 70,000$ . Powdered  $\text{In}_2\text{O}_3$  (99.99% Sigma-Aldrich) was added to PEDOT:PSS solution for some pH measurements at a concentration of 1.21 mg/mL.

For the solar cell active layers a binary all-polymer blend was used, consisting of poly((9,9-dioctylfluorene)-2,7-diyl-alt-[4,7-bis(3-hexylthiophen-5-yl)-2,1,3-benzothiadiazole]-2',2''-diyl) (F8TBT) supplied by Cambridge Display Technology Ltd. with a molecular weight ( $M_w$ ) of 55,000 and poly(3-hexylthiophene) (P3HT) supplied by Rieke Metals Inc. with a molecular weight ( $M_w$ ) of 46,000 and a regioregularity of 93% (electronic grade). The photoactive polymers were used without further purification. The P3HT:F8TBT system has been intensively studied previously in photodetector or photovoltaic applications [18,19] and in solar cells gave external quantum efficiencies up to 26% and power conversion efficiencies of 1.8% under solar simulator conditions [2].

### 2.2. Preparation

The PEDOT:PSS solutions were sonicated (10 min) before use. The solution heating was carried out in a metal hot block to ensure homogeneous heat distribution and the heated solutions were filtered with a preheated 0.25  $\mu\text{m}$  filter (Whatman PP w/GMF polypropylene membrane syringe filter with glass microfiber prefilter) before film deposition or solution characterization. Sonicated PEDOT:PSS solutions were modified by heating at temperatures between 20 °C and 90 °C for at least 10 min before further processing. The warm solutions were filtered and characterized either undiluted (pH value determination) or diluted (to a ratio of 1:50 for PEDOT:PSS) with water of the same temperature (dynamic light scattering). Undiluted, heated, filtered PEDOT:PSS solutions were deposited as thin films for further characterization (photovoltaic studies, conductivity, photoelectron spectroscopy, AFM, profilometer). This was done via spin-coating in ambient

air to yield a final thickness of about 70 nm. Note that the spin-coating chuck and substrate were at room temperature, so that the polymer solution cooled during spin-coating. The spin-cast samples were annealed at 230 °C while purged with dry N<sub>2</sub> gas (<1 ppm H<sub>2</sub>O) for 30 min to remove residual water. This temperature was found to be optimum for device performance in our previous study [11]. Samples were then cooled to room temperature in dry N<sub>2</sub> atmosphere and immediately sealed in separate small containers (additionally to glovebox storage) until further processing or measurement to avoid water or oxygen uptake. For conductivity determination gold channels with 80 μm channel width (sets of two parallel 3 mm-long gold stripes with a spacing of 80 μm) were evaporated (thickness: 50 nm) onto clean glass substrates, followed by deposition of PEDOT:PSS on top. For photoelectron spectroscopy studies (PEYS and XPS), the heated PEDOT:PSS solution was spun on fully covered ITO glass substrates. Profilometer and AFM imaging samples were prepared on Spectrosil quartz glass substrates. Photovoltaic devices were fabricated spinning a continuous layer of PEDOT:PSS on patterned ITO glass substrates. These were transferred to a nitrogen-filled glovebox for subsequent device fabrication steps. Firstly, the photoactive polymer layer was deposited on top by spin-coating from a 70 °C *o*-xylene solution of a 1:1 blend of P3HT:F8TBT (20 mg/mL) to give an active layer thickness of 70 nm. Then a 100 nm aluminum cathode was evaporated, followed by annealing of the device at 140 °C for 10 min. Finally devices were encapsulated with an epoxy-glass combination, prior to any air exposure and testing. All devices had an active area of 4.5 mm<sup>2</sup>.

### 2.3. Methods

Surface imaging was performed using atomic force microscopy (Veeco Dimension 3100 AFM) operated in tapping mode and with a probe tip of radius of curvature  $R_c < 10$  nm. Film thickness was measured using a stylus profilometer (Veeco Dektak 6 M). Monitoring of the pH values in solution was performed using a Jenway 370 pH meter, high-temperature-stable quartz-glass-bodied combination electrode and connected thermo element. The pH measurement was performed with automatic temperature compensation after two-point calibration. For device characterization, external quantum efficiency (EQE) was measured as a function of wavelength, using a monochromatic light source (250 W tungsten filament lamp, passed through a monochromator), with a final spot size smaller than the device active area. The short-circuit current was recorded with a Keithley 2635 source measure unit (SMU). Incident light intensity was continuously monitored during measurement and calibrated by a Thorlabs SM5PD1A photodiode. Current–voltage characteristics were recorded in the dark and under the same illumination as used for EQE measurements using the Keithley 2635 SMU. Current–voltage characteristics were also acquired under simulated solar conditions (intensity equivalent to 100 mW/cm<sup>2</sup>, AM 1.5 G, after correction for spectral mismatch) using a solar simulator light source (Oriel 81160-1000) calibrated to a silicon reference cell. The hydrodynamic diameter of particles

was determined by dynamic light scattering measurements using a Malvern Zetasizer. Measurements were performed on aqueous PEDOT:PSS solutions in the diluted regime (below overlap concentration). Two different concentrations, namely of 50 or 100 μg/ml were used to ensure independence of the data from solution concentration. Three independently prepared solutions were measured for each temperature with at least 20 runs each (number of runs was set by the Zetasizer software, dependent on the signal quality). The statistical particle size distribution for each measurement was calculated by the Malvern Zetasizer software. The program also takes temperature dependent parameters (e.g. solvent viscosity) into account. Resistance of the PEDOT:PSS films was measured under a N<sub>2</sub> atmosphere, using a two-point-probe setup on a Karl Suss probe station connected to an HP 4155B semiconductor parameter analyzer. The measurement was performed in-plane, across the PEDOT:PSS-covered evaporated 80 μm gold channel, by penetrating the polymer to make contact with the gold electrodes. XPS measurements were performed in an ultra-high-vacuum system with a Kratos Axis Ultra DLD XPS with a monochromated Al K<sub>α</sub> X-ray gun ( $h\nu = 1486.69$  eV) and a delay line detector. XPS data were analysed with CasaXPS (spectral data processing and analysis software). The core-level spectra were fitted with a combination of Gaussian and Lorentzian peaks after Shirley-background subtraction. Work functions were determined with photoelectron yield spectroscopy (PEYS) in air using a Riken-Keiki AC-2 surface analyzer (Riken Keiki Co., Ltd.). Full details of the AC-2 measurement can be found in the literature [20]. Briefly, film work function is determined by detecting the photoelectrons emitted from the film while the energy of incident UV light from a deuterium lamp (here operating at 250 nW) is varied between 4.5 and 6.2 eV with a monochromator. The work function is equal to the onset of photoelectron emission. For organic solids it is extracted from the linear fit of  $Y^{1/3}$  on a plot of  $Y^{1/3}$  versus  $h\nu$  since  $Y \sim (h\nu - W_f)^3$ , where  $Y$  is the photoelectron yield,  $h\nu$  the incident photon energy and  $W_f$  the material work function [21]. PEYS is advantageous compared to common UPS, because no vacuum is required and no charging of the sample occurs. Since also slower electrons are detected, the probing depth is 20–30 nm, much larger than for UPS (~10 nm), so surface effects have less impact on the measurement. This latter feature is useful to draw conclusions about the existence and thickness of thin dielectric surface layers on top of the samples from analysis of the yield slope [22]. If the photoelectron emission is retarded by such a damping surface layer, the slope will be smaller.

### 3. Results

For the investigation of heating effects on PEDOT:PSS solution and the consequences on solar cell performance we follow two different approaches. On the one hand physicochemical modifications occurring within the solution upon heating can be expected. On the other hand solution characteristics will affect the morphology and properties of solid thin films produced from such solutions via spin-coating. By examining in-depth the temperature

dependent properties of both solution and film, insight into the impact on photovoltaic device performance may be derived.

### 3.1. Effects on solution

One observation from PEDOT:PSS solution heating is the considerable change of particle size in solution, as determined by dynamic light scattering (DLS). Fig. 2a shows the distributions of hydrodynamic diameters in colloidal PEDOT:PSS solutions at various solution temperatures. We note that repeated measurements (as described in Section 2) yielded very similar distributions. It can be seen that the average particle size (Fig. 2b) remains stable at values of about 230 nm up to a solution temperature of 50 °C. With further heating from 60 °C up to 90 °C the particle size decreases rapidly to a new lower plateau at around ~40 nm, representing a size reduction of 83%. In thickness measurements on spun films for different solution temperatures we achieved similar values for all films of  $71 \pm 4$  nm, confirming the absence of significant alterations of the solid content of the filtered solutions [23,24]. We further found that the size alterations are reversible, with larger particles reforming in solution upon cooling. Associated effects occurring under spin-coating conditions will be discussed later.

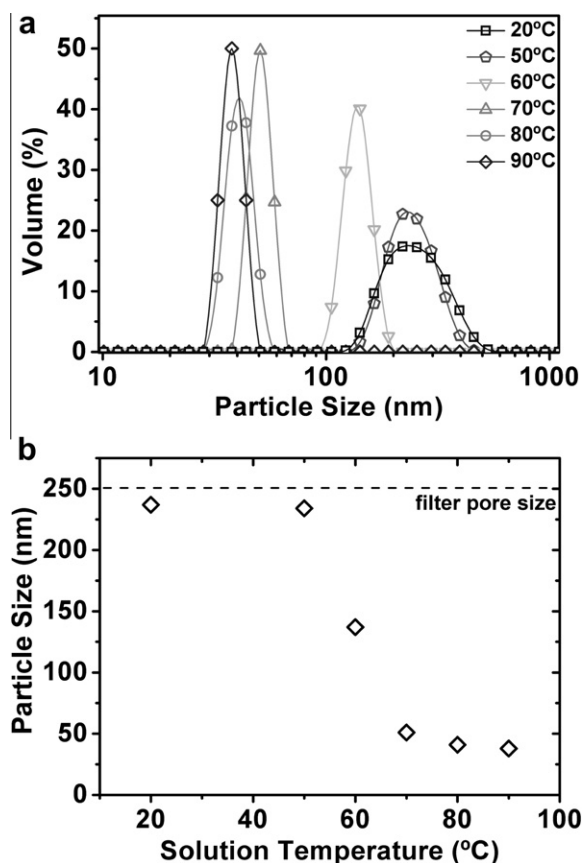


Fig. 2. Size distribution (a) and average particle diameters (b) in colloidal PEDOT:PSS solutions as a function of solution temperature as determined via dynamic light scattering.

Physicochemical processes in solution, especially in the presence of electrolytes like PSS, can be accompanied by changes in pH, since the concentration of hydrogen ions is affected. We found, however, no change in solution pH with heating, with a value of  $1.23 \pm 0.05$  measured independent of solution temperature (between 20 °C and 90 °C) and in agreement with specifications provided by the supplier of 1.2–1.8. Thus we can discount any temperature-induced ion exchanges involving hydrogen. We note that since solution deposition involves contact with the ITO electrode, there may be a corrosive interaction during the brief spin-coating period before the film dries. To exclude any ITO-induced change in pH we have also measured the pH of PEDOT:PSS solutions with  $\text{In}_2\text{O}_3$  powder added. A concentration of 1.21 mg/mL was used to simulate the maximum likely concentration of dissolved  $\text{In}_2\text{O}_3$  in a 60  $\mu\text{l}$  solution that is dispensed onto an ITO electrode (dimensions of ITO stripe: 12 mm  $\times$  7 mm  $\times$  120 nm) during spin-coating. However, we saw no change in pH with  $\text{In}_2\text{O}_3$  added, remaining at  $\text{pH } 1.23 \pm 0.05$  independent of temperature. We note that this is contrast to the results of Chang and Chen [25], who observed an increase in pH value by adding  $\text{In}_2\text{O}_3$  to PEDOT:PSS solution at room temperature, however the reaction was observed to take several hours, much longer than the time window of a few minutes used here to mimic spin-coating conditions. These observations show that whatever reactions may take place between PEDOT:PSS and ITO (such as the release of indium into the PEDOT:PSS solution), they do not significantly affect the concentration of the hydrogen ions.

### 3.2. Effects on films

We firstly look for possible chemical modifications of films spin-coated at different solution temperatures with X-ray photoelectron spectroscopy. Having a probing depth of less than 10 nm, XPS is used to quantify the elemental surface composition and provides information about the chemical environment. Survey scans covering binding energies of 0–1400 eV were first performed to identify elements in the film, with significant amounts of sodium (1070 eV), oxygen (532 eV), indium (446 eV), carbon (284 eV) and sulfur (170 eV) found. As discussed above, the presence of indium is most likely caused by diffusion of indium ions induced by the high acidity of the PEDOT:PSS solution [26]. Sodium is a trace component in PEDOT:PSS solutions (here less than 400 ppm after ion-exchange purification, as stated by the supplier), caused by the preparation process, involving  $\text{Na}^+\text{PSS}^-$ . The nominal concentrations of the elements detected near the surface of a standard room temperature spun PEDOT:PSS film were: 1.1% sodium (Na 1s), 19.3% oxygen (O 1s), 1.8% indium (In 3d), 70.6% carbon (C 1s) and 7.2% sulfur (S 2p). A comparison between sample films spun from differently heated solutions showed slightly varying compositions (changes <2%), but no obvious trends. High-resolution scans of oxygen (O 1s) and sulfur (S 2p) peaks were recorded to check for any changes in chemical environment of these two elements, which are of specific interest for PEDOT:PSS, such as changes in chemical bonds [8,27]. According to the work of Greczynski et al. [5] the sulfur

and oxygen peaks of PEDOT:PSS may have multiple components originating from PEDOT, PSSH and  $\text{PSS}^- \text{Na}^+$  species that all have slightly shifted characteristic energies. The sulfur and oxygen core-level spectra for our PEDOT:PSS films spun from solutions heated between 20 °C and 90 °C are shown in Fig. 3.

The sulfur spectra obtained (Fig. 3a) are all consistent with one chemical species, namely the PSSH doublet located at 169.9 eV ( $\text{S } 2p_{1/2}$ ) and 168.7 eV ( $\text{S } 2p_{3/2}$ ). No indications of  $\text{PSS}^- \text{Na}^+$  or PEDOT were found. We note that the effective energy values slightly differ from those reported in literature [5], which may result from the calibration of the spectrometer. We did not observe any change in the sulfur core-level spectra with heating of the PEDOT:PSS solutions. Analysis of the oxygen core-level spectra (Fig. 3b) showed only two contributions; one is attributed to oxygen–sulfur double bonds (O=S) in the sulfonate group in PSSH at 532.2 eV and the other to hydroxyl groups (O–H) at 533.4 eV from PSSH and residual water [5]. The hydroxyl peak appears to be rather broad, possibly caused by hydroxyl groups participating in hydrogen bonds [5]. A peak intensity ratio between O–H bonds and O=S bonds of 1:9 was observed (measured composition 10.5% O–H and 89.5% O=S). We suggest that the comparatively low amount of O–H bonds is mainly caused by our post-deposition film annealing at 230 °C, which firstly might have removed most inter- and intra-particle water and additionally condensated (dehydrolysed) a large quantity of the existing hydroxyl groups in the solid film. No further contributions of either  $\text{PSS}^- \text{Na}^+$  or PEDOT were found. Just as for the sulfur, no significant changes between the films spun from solution at different temperatures were observed in the oxygen core-level spectra. It should be mentioned that our 230 °C film annealing step is below the temperature at which the rupture of the sulfonate group from PSS takes place [5,11]. This has been supported by further XPS studies which we have performed on PEDOT:PSS films annealed at temperatures between 140 °C and 300 °C in  $\text{N}_2$  (graphs not shown). Only for films annealed above 260 °C we could observe additional contributions due to the presence of PEDOT at the surface (at 165.4 eV ( $\text{S } 2p_{1/2}$ ), 164.2 eV ( $\text{S } 2p_{3/2}$ ) and 533.6 eV (O 1s)) and an energy-shift in the PSS sulfur doublet, indicating the predominance of  $\text{PSS}^- \text{Na}^+$  due to PSSH degradation. Both effects were already reported in the literature [5].

For most optoelectronic applications, as in organic photovoltaic devices, the work function of the electrode is crucial and can be one of the factors limiting performance. We have therefore determined the work function changes of films spun from PEDOT:PSS solutions heated at different temperatures via (ultraviolet) photoelectron yield spectroscopy (PEYS). Additionally the yield slopes have been analyzed which can indicate an increase or decrease in the thickness of dielectric surface layers such as excess PSS. Fig. 4a shows the baseline-corrected plots of the photoelectron yield  $Y^{1/3}$  plotted against photon energy for different solution temperatures.

At first sight the absence of obvious onset shifts or changes of slope implies that there are only subtle differences upon variation of solution temperature. The work function values and slopes, obtained from linear fits to  $Y^{1/3}$ , are displayed in Fig. 4b. Despite the comparatively high experimental uncertainty of the measurement ( $\Delta W_f = \pm 0.05$  eV), there appears to be a trend in the work function development with solution temperature. Up to 70 °C the work function  $W_f$  remains at a stable value of around 5.38 eV; with higher solution temperatures it increases up to 5.50 eV for the 90 °C sample. The slopes of the photoemission yield curves, which represent a measure of the photoelectron emission rates, do not follow the same trend. The highest emission rate within the studied temperature range was found for films spun from room-temperature solution. With increasing solution temperature the emission rate drops, with a minimum for the 70 °C sample. Temperatures above 70 °C cause rising emission rates (higher slopes) from the films. This could be an indication for a variation in thickness of the excess PSS surface layer with solution temperature or changing film density. It should be noted that the short exposure to air during the measurement might have slightly influenced the data due to the strongly hygroscopic nature of PSS. However, apart from a control sample that had been exposed to air for several hours, none of the films shows signs of strong water uptake, which is typically reflected by a strongly lowered work function of around 5.05 eV [6,7,28].

Conductivity is likely to be one of the most important characteristics of an electrode material in a solar cell. PEDOT:PSS films were spun from solutions at different temperatures and subsequently annealed for conductivity measurement. The corresponding development of in-plane conductivity with solution temperature is shown in Fig. 5.

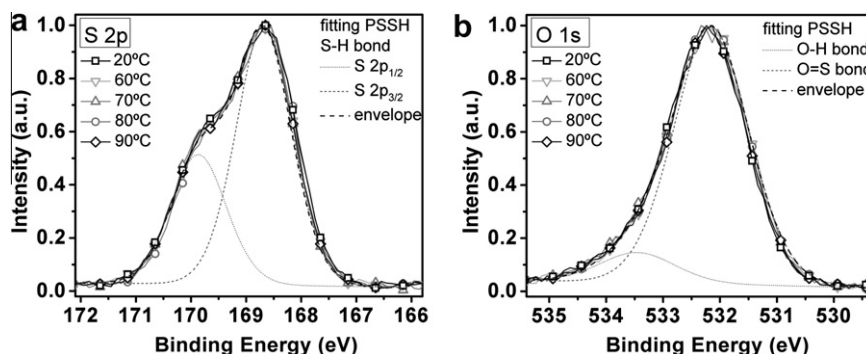
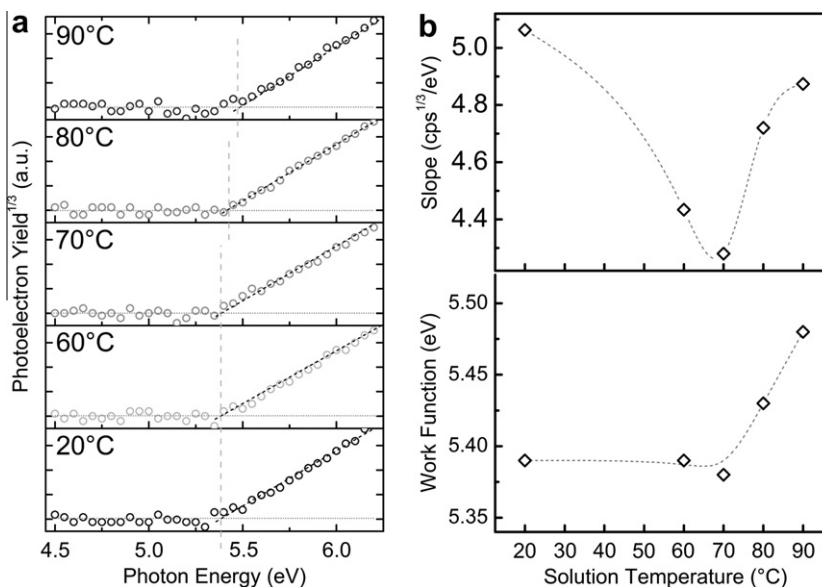
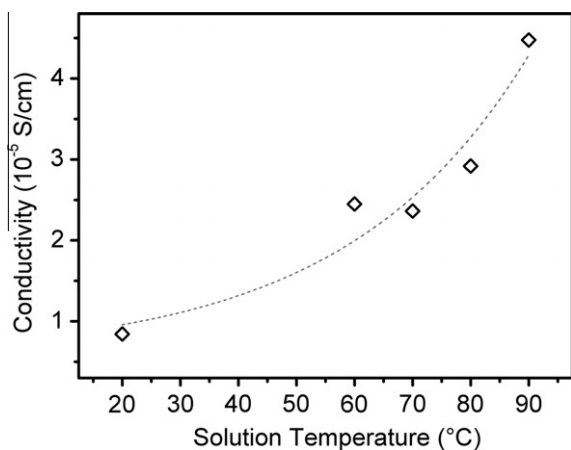


Fig. 3. (a) Sulfur ( $\text{S } 2p$ ) and (b) oxygen ( $\text{O } 1s$ ) XPS core-level spectra of PEDOT:PSS films spun from differently heated solutions.



**Fig. 4.** (a) Cube root plot of the photoelectron yield from PEDOT:PSS films prepared from heated solution. (b) Slope extracted from linear fit to yield (top) and measured work function (bottom) as a function of PEDOT:PSS solution temperature (the dashed lines are a guide to the eye).



**Fig. 5.** In-plane conductivity of equally annealed PEDOT:PSS films spun from differently heated aqueous colloidal PEDOT:PSS solutions (the dashed line is meant as guide to the eye).

We found that the in-plane bulk conductivity is enhanced by a factor of five with increasing solution temperature from 20 °C to 90 °C. This is in good agreement with results reported by Tsai et al. [29], who found 2–3 times higher conductivity in films spun from PEDOT:PSS solutions heated from 20 to 160 °C.

The morphology of PEDOT:PSS solid films, spun from solution at different temperatures has been investigated with AFM. Fig. 6a shows the height images for PEDOT:PSS films spun from heated solutions between 20 °C and 90 °C, after subsequent annealing.

It is apparent that although the macroscopic roughness of all films is very similar, there is a refinement in the microscopic structure for films spun at 60 °C and higher. There are obviously considerable changes in particle dimension depending on the PEDOT:PSS solution temperature. The

average particle size (Fig. 6b), as acquired from statistical feature size analysis of AFM cross-sectional line scans of the different films, reveals a trend similar to that one seen from DLS on PEDOT:PSS solutions (Fig. 2b). The feature size remains stable at about 55 nm for films up to 50 °C solution temperature and then drops quickly for higher temperatures to a new plateau at around 20 nm. It should be mentioned that a further size decrease might not be detectable as AFM resolution is limited by the tip size ( $R_C < 10$  nm).

### 3.3. Effects on solar cells

Finally the effect of PEDOT:PSS solution temperature on the performance of P3HT:F8TBT solar cells has been studied. Fig. 7 plots external quantum efficiency *EQE* (Fig. 7a), current–voltage characteristics under solar simulator conditions (AM1.5G) (Fig. 7b) and specific key solar cell parameters (Fig. 7c) (namely short-circuit current density,  $J_{sc}$ , open-circuit voltage,  $V_{oc}$ , fill factor, *FF*, and power conversion efficiency,  $\eta$ ) as a function of PEDOT:PSS solution temperature. As expected, the *EQE* curves (Fig. 7a) do not show any significant spectral change since the active layer is kept constant. However, there are variations in the magnitude of *EQE* with maximum *EQE* increasing with increasing PEDOT:PSS solution temperature to a maximum at 70 °C, then falling again as temperature is increased to 90 °C. A similar trend is seen in the current–voltage characteristics. Fig. 7c shows that all key parameters are optimized with a solution temperature of 70 °C, which is most apparent for  $J_{sc}$  and  $\eta$ , while  $V_{oc}$  and *FF* only change slightly.

## 4. Discussion

Among the numerous publications addressing the optimization of PEDOT:PSS films for use in organic

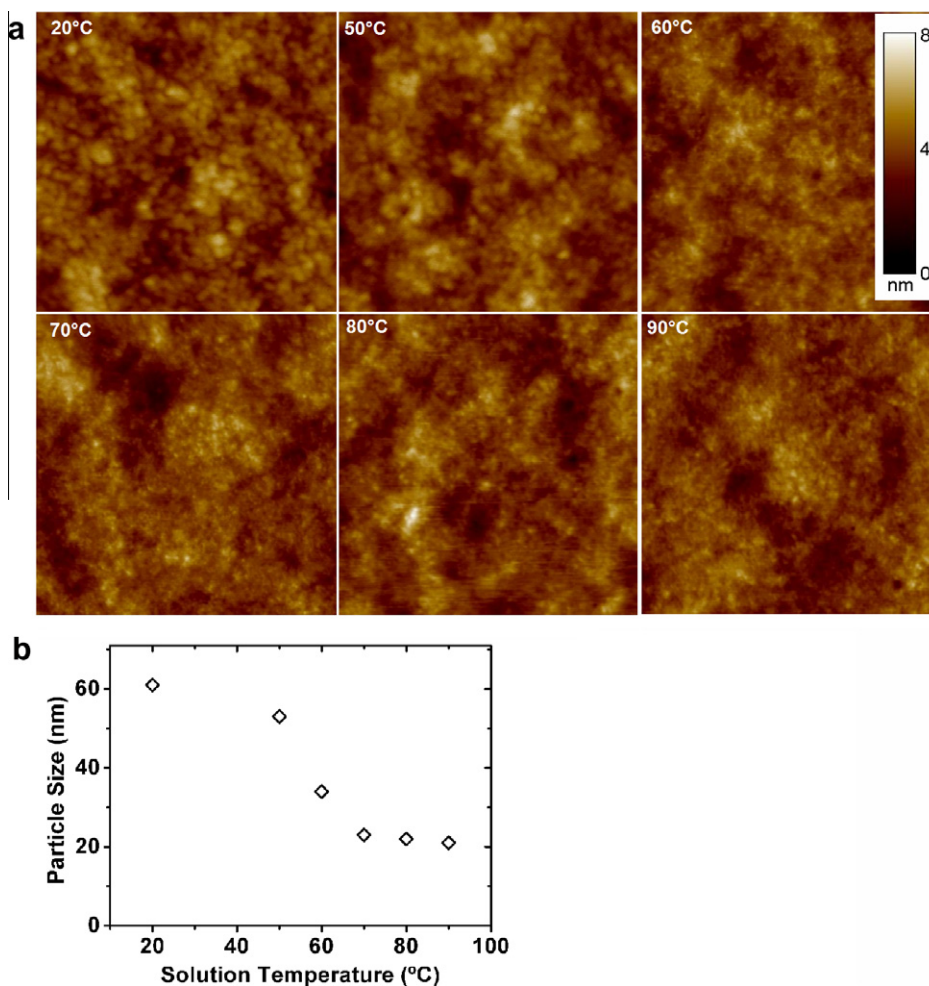


**Fig. 6.** (a) AFM height images ( $2\ \mu\text{m} \times 2\ \mu\text{m}$ ) of the surface morphology for PEDOT:PSS films spun from heated solutions. (b) Temperature dependent development of average feature size in these films.

optoelectronic devices, changes in particle/grain size by addition of dopants or co-solvents, have occasionally been addressed. Usually these have been attributed to agglomerate formation [30–32], e.g. due to dominating Van-der-Waals forces facilitated by partial removal of the repulsive negatively charged surface PSS layer (e.g. by solvent additives) [33]. We found in our experiments that the size variations could be detected within a few minutes in highly diluted solutions. This makes agglomeration as a cause for a size increase unlikely, since the required diffusion processes for interparticle contacts take place on a much longer time scale (days or weeks). Furthermore the particles could not be broken down by ultrasonication, which also speaks against agglomeration effects. We suggest that the observed solution-temperature-induced size effects are rather associated with the phase behavior of PEDOT:PSS, which has not been reported in this context so far.

The solubility of PEDOT:PSS in aqueous solution is mainly determined by the presence of the charged sulfonate groups on the polystyrene backbone, since PEDOT and polystyrene are both hydrophobic on their own. Exper-

imental and theoretical approaches reported in literature have shown that phase behavior of PSS crucially depends on the degree of sulfonation, the distribution of the sulfonate groups along the backbone, the presence and strength of counter ions or the presence of salts in solution [34–37], information which was not fully available, either for commercial PSS solution or for the PSS used in PEDOT:PSS, making it difficult to compare the two systems. Although some values could have been determined experimentally, that is beyond the scope of this publication.

The size dependence of NaPSS with temperature has been the subject of only few earlier studies, finding an increase of hydrodynamic size of the chains with increasing solution temperature from 5 nm up to 18 nm and demixing with an upper critical solution temperature (UCST) [38,34]. Fig. 2 shows an opposite trend, with a decrease in size of PEDOT:PSS particles with increasing solution temperature. This indicates phase separation of the polymer solution at high solution temperatures. Microscopically this means that the polymer chains are most extended at low temperatures and contract/collapse towards higher temperatures. A phase behavior of this kind is typical for a lower critical

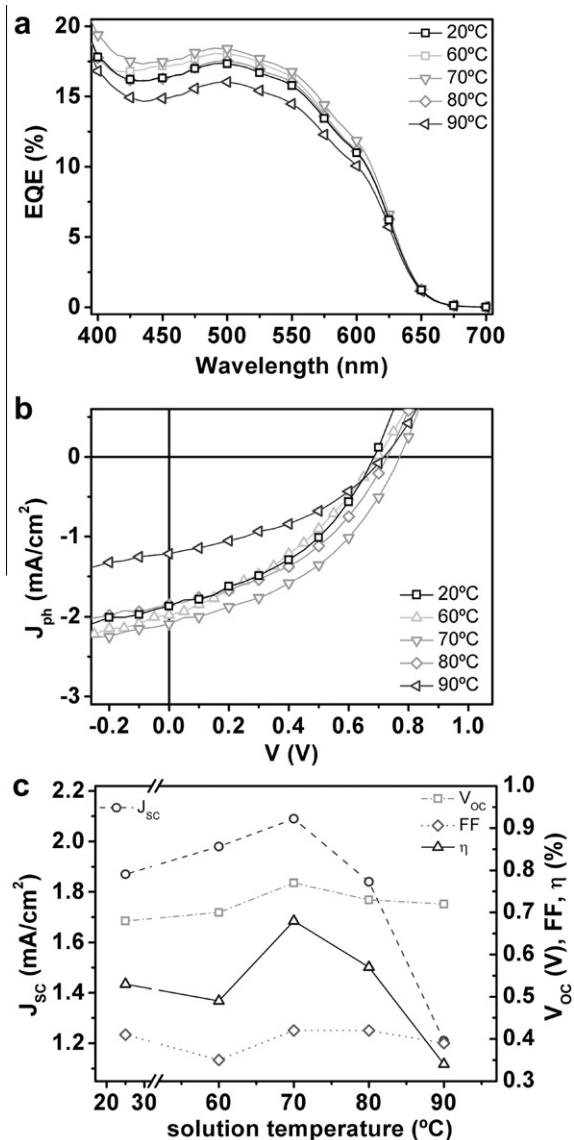


**Fig. 7.** Characteristics of solar cell devices with PEDOT:PSS films spun from differently heated PEDOT:PSS solutions, (a) external quantum efficiency, (b) photocurrent density (AM1.5G) and (c) key photovoltaic parameters.

solution temperature (LCST), similar to the phase behavior of other polymer solutions [39a]. The variation of particle size in the dry PEDOT:PSS films shows a very similar behavior. Although this trend could also arise from the change of other solution parameters during spin-coating, the similarity of Figs. 2b and 6b suggests the dominance of an LCST behavior of PEDOT:PSS on the particle size in the film. Fig. 8 summarizes the two data sets and schematically indicates the trajectories in phase space of the two experiments. Heating a solution at fixed concentration is indicated by the red dashed (vertical) arrow. Phase separation occurs when the trajectory crosses the binodal line (boundary between polymer–solvent miscibility and immiscibility). In a dilute solution this is accompanied by a step decrease in the hydrodynamic diameter, as observed

in the DLS experiments (Fig. 8, right), caused by a collapse of the polymer chains. This process is fully reversible. Spin-coating, on the other hand ideally occurs at constant temperature. Solvent evaporation increases the solution concentration, indicated by the blue dashed (horizontal) arrow in the phase diagram. Horizontally crossing the binodal gives rise to a similar step in particle size, as observed in the as-cast films (Fig. 8, left). In practice, the trajectory for spin-coating from heated solutions is slightly more complex. In addition to a rapid concentration change, the temperature also changes, by casting the solution onto a cold substrate and through evaporative cooling. While this implies a diagonal trajectory in the phase diagram (indicated by the purple (diagonal) arrows), the description for the ideal spin-coating process remains qualitatively valid. Both trends for the hydrodynamic and solid diameter agree well with this scenario. Preheating the substrates, while feasible, substantially changes the evaporation rate of the solution, possibly causing additional changes in the films. The very similar cross-over temperatures of the two data sets in Fig. 8 suggest, however, that film formation occurs much more quickly than a change in particle size. This is in agreement with recent results showing a very slow change in the conformation of polymer brushes upon crossing a LCST [39b].

A further interesting observation arises from the comparison of Figs. 2b and 6b. The particle diameter decreased from 230 nm in solution to 55 nm in the film (i.e. by a factor of 4) when the casting from a 20 °C solution, compared to a size change from 40 nm to 20 nm (by a factor of 2) when the spin coating was above 70 °C. This observation indicates that the coils were less swollen in solution at the high temperatures compared to room temperature, in good agreement with the LCST assumption mentioned above. This result also matches well recent non-equilibrium effects in spin-cast polystyrene films reported by Thomas et al. [40], showing that that solution coil conformations are substantially preserved in the film after spin-coating [41].

In the case of the PEDOT:PSS micellar solution, the signature of an LCST behavior is as follows: Because most PSS chains are localized around PEDOT cores, the phase transition leads to a change in micellar size, which leads to the observations in Fig. 8. Secondly macroscopic phase separation of the suspension into polymer-rich and polymer-poor phases should set in at high temperatures. This second process, which is much slower (on the time scale of many hours), was not investigated in detail.

LCST phase behavior of polymer solutions is less common than the UCST type, but often occurs for polymers that can form hydrogen bonds with the solvent [42]. In the case of PEDOT:PSS the presence of hydrogen bridges between sulfonate groups has been reported [31], which could be responsible for the observed LCST phase behavior. It is worth mentioning that hydrated PSS-chains are to some degree extended into the aqueous medium, while they are fully collapsed in the dry film. Macroscopically this is observed when swollen particles in solution shrink during drying, leading to the reported dried PEDOT:PSS grains with PEDOT-rich core, covered by a thin insulating PSS layer [37,38].

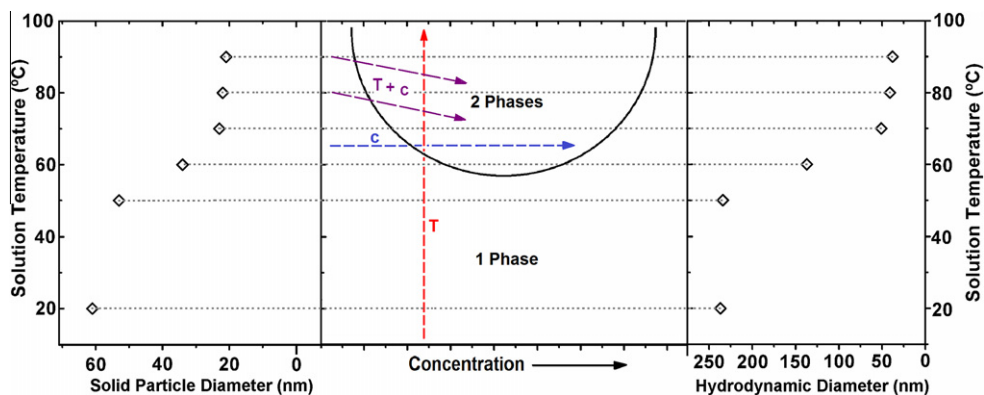


**Fig. 8.** Schematic LCST-phase diagram illustrating trajectories of solution heating and spin-coating, associated with the obtained trends of average particle diameters as determined from DLS from PEDOT:PSS colloidal solutions (right) and in solid films (left) as a function of solution temperature.

We did not observe any variation in pH value of the PEDOT:PSS solution during heating, neither in pure solution nor involving indium oxide. This is not indicative of PEDOT:PSS-induced ITO corrosion during film formation, which is suspected to cause damage of the organic active layer by indium diffusion already during device fabrication.

The temperature-induced shrinkage of the PEDOT:PSS particles was accompanied by a considerable effect on the film conductivity which was quadrupled by solution heating. It has been reported that smaller PEDOT:PSS particles actually cause lower film conductivity [12], since PEDOT:PSS conductivity is determined by the extension of the conducting PEDOT-rich domains and the hopping distance/frequency across the insulating PSS phases. We found that the interface properties are characterized by an increasingly refined structure and densification of the PEDOT:PSS film, leading to shorter hopping distance between the conductive PEDOT-rich units, the consequence of which is a lower bulk resistance and enhanced interlayer contact.

However, the fact that even for small particles the PSS-shell is at least 10 nm thick, explains why no PEDOT was detected from the films via XPS within the nominal probing depth of 10 nm, independent of the solution temperature. Nor was any other evidence for chemical changes found near the surface.

The observed increase in film work function for solutions exceeding 70 °C is probably caused by the densification of the film causing considerable changes in the interface properties. Even more significant is the behavior of the photoelectron emission rates, represented by the yield slope. The rate starts at a high level, because for low solution temperatures the films are porous and in spite of the thicker damping PSS shell surrounding the particles, more electrons can be detected. When the film density grows towards 70 °C, the rates go down, due to increasingly hindered signal from the depth of the film. Exceeding 70 °C, the emission rates raise again, because the dimensions of the PSS shell of the particles are significantly reduced.

When films from solution-heated PEDOT:PSS are incorporated into a P3HT:F8TBT solar cell, we find that actually

most of the key characteristics peak at a PEDOT:PSS solution temperature of 70 °C. It seems obvious that the largest improvement is caused by the enhanced conductivity of the PEDOT:PSS films. However, it is still questionable why the PV performance does not improve beyond 70 °C while the conductivity is still rising. Possible reasons include changes in work function or other interface properties, and changes in vertical charge transport (as opposed to the lateral conductivity measured here). Although the observed work function shift is not large ( $\Delta W_f = 0.1$  eV), it could be just sufficient to form a barrier for hole extraction from P3HT. Accordingly the performance would go down for higher solution temperatures. It has been reported earlier [43], that vertical charge transport in PEDOT:PSS can be up to three orders of magnitude lower than in-plane, due to layers of segregated excess PSS. Though we cannot prove this by our spectroscopic or imaging data, it is possible that the phase transitions seen in PEDOT:PSS are accompanied by alterations of the amount of electrostatically bound excess PSS. In that case the release or withdrawal of free PSS into/from solution could certainly change the presence and extension of insulating horizontal PSS interlayers in the resulting films.

## 5. Conclusions

In this work, the influence of heating on PEDOT:PSS colloidal solutions and its consequence on the performance of polymer–polymer photovoltaic devices has been investigated. We found reversible heat-induced reduction in size of PEDOT:PSS particles by solution heating between 20 °C and 70 °C. We associated this transition with LCST-type phase behavior of PEDOT:PSS. This transition from large particles with a thicker (expanded) insulating PSS-shell to smaller particles covered with a thin (contracted chains) PSS layer causes property alterations in resulting films. In particular, increasing the solution temperature results in films with finer structure, higher density, increased conductivity and work function. Solar cell performance was found to improve, but only up to 70 °C. Above 70 °C, device performance deteriorated alongside an increase in PEDOT:PSS work function, suggesting the formation of a hole

extraction barrier. Based on our observations, we conclude that PEDOT:PSS solutions heated at 70 °C deliver the most beneficial film properties for P3HT:F8TBT solar cells. These results may have implications in the roll-to-roll manufacture of organic photovoltaics, where the liquid film deposited by printing is heated to aid drying [44,45]. Changes in PEDOT:PSS particle size during this process may have a direct impact on device performance.

## Acknowledgment

We are grateful to Cambridge Display Technology Ltd. (CDT) for the supply of materials, to the Technology Strategy Board for funding, as part of the OPALS (TP/K2512F) collaborative project with CDT and Molecular Vision Ltd., and to Dr. J.J.M. Halls, Dr. R.J. Wilson and Dr. A.B. Doust for useful discussions. T.J.K.B. and C.R.M. thank the EPSRC for support through Grant no. EP/E051804/1.

## References

- [1] A.C. Mayer, S.R. Scully, B.E. Hardin, M.W. Rowell, M.D. McGehee, *Mater. Today* 10 (2007) 28–33.
- [2] C.R. McNeill, J.J.M. Halls, R. Wilson, G.L. Whiting, S. Berkebile, M.G. Ramsey, R.H. Friend, N.C. Greenham, *Adv. Funct. Mater.* 18 (2008) 2309–2321.
- [3] Y. Liang, Z. Xu, J. Xia, S.T. Tsai, Y. Wu, G. Li, C. Ray, L. Yu, *Adv. Mater.* 22 (2010) E135–E138.
- [4] H.Y. Chen, J.H. Hou, S.Q. Zhang, Y.Y. Liang, G.W. Yang, Y. Yang, L.P. Yu, Y. Wu, G. Li, *Nat. Photonics* 3 (2009) 649–653.
- [5] G. Greczynski, T. Kugler, M. Keil, W. Osikowicz, M. Fahlman, W.R. Salaneck, *J. Electron Spectrosc. Relat. Phenom.* 121 (2001) 1–17.
- [6] A.M. Nardes, M. Kemerink, M.M. de Kok, E. Vinken, K. Maturova, R.A.J. Janssen, *Org. Electron.* 9 (2008) 727–734.
- [7] J.S. Huang, P.F. Miller, J.S. Wilson, A.J. de Mello, J.C. de Mello, D.D.C. Bradley, *Adv. Funct. Mater.* 15 (2005) 290–296.
- [8] T.P. Nguyen, S.A. de Vos, *Appl. Surf. Sci.* 221 (2004) 330–339.
- [9] E. Vitoratos, S. Sakkopoulos, E. Dalas, N. Paliatsas, D. Karageorgopoulos, F. Petraki, S. Kennou, S.A. Choulis, *Org. Electron.* 10 (2009) 61–66.
- [10] Y. Kim, A.M. Ballantyne, J. Nelson, D.D.C. Bradley, *Org. Electron.* 10 (2009) 205–209.
- [11] B. Friedel, P.E. Keivanidis, T.J.K. Brenner, A. Abrusci, C.R. McNeill, R.H. Friend, N.C. Greenham, *Macromolecules* 42 (2009) 6741–6747.
- [12] S. Kirchmeyer, K. Reuter, *J. Mater. Chem.* 15 (2005) 2077–2088.
- [13] X. Crispin, S. Marciniak, W. Osikowicz, G. Zotti, A.W.D. Van der Gon, F. Louwet, M. Fahlman, L. Groenendaal, F. De Schryver, W.R. Salaneck, *J. Polym. Sci. Pt. B-Polym. Phys.* 41 (2003) 2561–2583.
- [14] M. Kemerink, S. Timpanaro, M.M. de Kok, E.A. Meulenkaamp, F.J. Touwslager, *J. Phys. Chem. B* 108 (2004) 18820–18825.
- [15] S.G. Im, E.A. Olivetti, K.K. Gleason, *Surf. Coat. Technol.* 201 (2007) 9406–9412.
- [16] J. Hwang, F. Amy, A. Kahn, *Org. Electron.* 7 (2006) 387–396.
- [17] C.R. McNeill, A. Abrusci, J. Zaumseil, R. Wilson, M.J. McKiernan, J.H. Burroughes, J.J.M. Halls, N.C. Greenham, R.H. Friend, *Appl. Phys. Lett.* 90 (2007) 193506.
- [18] B. Friedel, C.R. McNeill, N.C. Greenham, *Chem. Mat.* 22 (2010) 3389–3398.
- [19] T.J.K. Brenner, I. Hwang, N.C. Greenham, C.R. McNeill, *J. Appl. Phys.* 107 (2010) 114501.
- [20] H. Kirihiata, M. Uda, *Rev. Sci. Instrum.* 52 (1981) 68–70.
- [21] Y. Nakayama, S. Machida, T. Minari, K. Tsukagishi, Y. Noguchi, H. Ishii, *Appl. Phys. Lett.* 93 (2008) 173305.
- [22] T. Kagiya, Y. Saito, K. Otobe, S. Nakajima, *Appl. Surf. Sci.* 216 (2003) 542–548.
- [23] Y.J. Min, M. Akbulut, K. Kristiansen, Y. Golan, J. Israelachvili, *Nat. Mater.* 7 (2008) 527–538.
- [24] G.V. Franks, *Chem. Eng. Res. Des.* 83 (2005) 937–945.
- [25] C.H. Chang, S.A. Chen, *Appl. Phys. Lett.* 91 (2007) 103514.
- [26] M.P. de Jong, L.J. van Ijzendoorn, M.J.A. de Voigt, *Appl. Phys. Lett.* 77 (2000) 2255–2257.
- [27] G. Greczynski, T. Kugler, W.R. Salaneck, *Thin Solid Films* 354 (1999) 129–135.
- [28] N. Koch, A. Vollmer, A. Elschner, *Appl. Phys. Lett.* 90 (2007) 043512.
- [29] K.H. Tsai, S.C. Shiu, C.F. Lin, *Proc. SPIE* 7052 (2008) 70521B.
- [30] H.J. Snaith, H. Kenrick, M. Chiesa, R.H. Friend, *Polymer* 46 (2005) 2573–2578.
- [31] U. Lang, E. Muller, N. Naujoks, J. Dual, *Adv. Funct. Mater.* 19 (2009) 1215–1220.
- [32] H. Yan, S. Arima, Y. Mori, T. Kagata, H. Sato, H. Okuzaki, *Thin Solid Films* 517 (2009) 3299–3303.
- [33] H. Yan, H. Okuzaki, *Synth. Met.* 159 (2009) 2225–2228.
- [34] S. Kanai, M. Muthukumar, *J. Chem. Phys.* 127 (2007) 244908.
- [35] A.V. Dobrynin, M. Rubinstein, *Prog. Polym. Sci.* 30 (2005) 1049–1118.
- [36] J.M.Y. Carrillo, A.V. Dobrynin, *J. Phys. Chem. B* 114 (2010) 9391–9399.
- [37] S. Block, C.A. Helm, *J. Phys. Chem. B* 112 (2008) 9318–9327.
- [38] E. Serhatli, M. Serhatli, B.M. Baysal, F.E. Karasz, *Polymer* 43 (2002) 5439–5445.
- [39] [a] I. Teraoka, *Polymer Solutions: An Introduction to Physical Properties*, John Wiley & Sons, 2002; [b] R. Poets, PhD Thesis, University of Cambridge 2010.
- [40] K.R. Thomas, A. Chenneviere, G. Reiter, U. Steiner, *Phys. Rev. E* 83 (2011) 021804.
- [41] D.R. Barbero, U. Steiner, *Phys. Rev. Lett.* 102 (2009) 248303.
- [42] T. Tsubouchi, K. Nishida, T. Kanaya, *Colloids and Surfaces B: Biointerphases* 56 (2007) 265–269.
- [43] A.M. Nardes, M. Kemerink, R.A.J. Janssen, *Phys. Rev. B* 76 (2007) 085208.
- [44] F.C. Krebs, T. Tromholt, M. Jørgensen, *Nanoscale* 2 (2010) 873.
- [45] F.C. Krebs, S.A. Gevorgyan, J. Alstrup, *J. Mater. Chem.* 19 (2009) 5442–5451.